Highly sensitive and ultrastable skin sensors for biopressure and bioforce measurements based on hierarchical microstructures

Highly Sensitive and Ultra-Stable Skin-Sensors for Bio-Pressure and Bio-Force Measurements Based on Hierarchical Microstructures

Journal:	*ACS Applied Materials & Interfaces*
Manuscript ID	am-2017-16611n
Manuscript Type:	Article
Date Submitted by the Author:	01-Nov-2017

Complete List of Authors:	Sun, Qi-Jun; City University of Hong Kong, Physics&Materials Science Zhuang, Jiaqing; City University of Hong Kong, Physics and Materials Science Venkatesh, Shishir; City University of Hong Kong, Physics Zhou, Ye; Shenzhen University, Institute for Advanced Study Han, Su-Ting; Shenzhen University, Department of Microelectronics College of Electronics Science & Technology Wu, Wei; City University of Hong Kong, Department of Physics and Materials Science Kong, Ka-Wai; City University of Hong Kong, Physics&Materials Science Li, Wen Jung; City University of Hong Kong, Department of Mechanical and Biomedical Engineering Chen, Xianfeng; The University of Edinburgh Li, Robert; City University of Hong Kong, Physics & Materials Science Roy, Vellaisamy A. L.; City University of Hong Kong, Materials Science and Engineering

Highly Sensitive and Ultra-Stable Skin-Sensors for Bio-Pressure and Bio-Force Measurements Based on Hierarchical Microstructures

*Qi-Jun Sun[a], Jiaqing Zhuang[a], Shishir Venkatesh[a], Ye Zhou[b], Su-Ting Han[c], Wei Wu[a], Ka-Wai Kong[d], Wen-Jung Li[d], Xianfeng Chen[e], Robert K. Y. Li[a], and Vellaisamy A. L. Roy[a]**

[a]Department of Materials Science and Engineering, City University of Hong Kong, Tat Chee Avenue, Kowloon, Hong Kong SAR, China.

[b]Institute for Advanced Study, Shenzhen University, Shenzhen 518060, P. R. China.

[c]College of Electronic Science and Technology, Shenzhen University, Shenzhen 518060, P. R. China.

[d]Department of Mechanical and Biomedical Engineering, City University of Hong Kong, Tat Chee Avenue, Kowloon, Hong Kong SAR, China.

[e]Institute for Bioengineering, School of Engineering, The University of Edinburgh, United Kingdom.

KEYWORDS

Highly sensitive, Bio-inspired, E-skin, Healthcare monitoring, Phonation rehabilitation

ABSTRACT

Piezoresistive microsensors are considered to be essential components of the future wearable electronic devices. However, the expensive cost, complex fabrication technology, poor stability,

and low yield have limited their developments for practical applications. Here we present a cost-effective, relatively simple, and high-yield fabrication approach to construct highly sensitive and ultra-stable Piezoresistive sensors using a bio-inspired hierarchically structured graphite/polydimethylsiloxane (PDMS) composite as the active layer. In the fabrication, a commercially available sandpaper is employed as the mold to develop the hierarchical structure. Our devices exhibit fascinating performance including an ultra-high sensitivity (64.3 kPa^{-1}), fast response time (< 8 ms), low limit of detection (LOD) of 0.9 Pa, long-term durability (> 100,000 cycles) and high ambient stability (> 1 year). The applications of these devices in sensing radial artery pulses, acoustic vibrations, and human body motion are demonstrated, exhibiting their enormous potential use in real-time healthcare monitoring and robotic tactile sensing.

INTRODUCTION

Flexible Piezoresistive sensors with high sensitivity, excellent stability, and low operating voltage have attracted tremendous attention due to their potential applications in medical diagnostics, artificial skin, and touch-on displays.[1-6] In general, most of the reported Piezoresistive sensors are based on assessing changes in capacitance,[2,7-14] resistivity,[15-26] and piezoelectricity[27,28] in response to external pressure. Among these three configurations, piezoresistive device, which transduces the external pressure into corresponding output electrical resistance, has been widely investigated because of its simple device structure and required circuit for data acquisition. Recently, great efforts have been paid to enhance the responsivity, sensitivity, frequency response, and workable pressure range of Piezoresistive sensors through material optimization and excellent structural design.[6,13,19,24,29-37] Remarkably, it has been demonstrated that, in the fabrication of Piezoresistive sensors, patterning the surface of the sensing layer with microstructures is an effective approach to obtain a high sensitivity and a low detection limit.[2,15,25,38-41] For example, the sensitivity of a capacitive pressure sensor based on microstructured PDMS film exhibited about 30 times higher than that of the unstructured one in the same pressure range.[2] Additionally, the relaxation time of the Piezoresistive sensor with microstructured PDMS film was about 1000 times faster than that fabricated on unstructured film.[2] However, the microstructures were mainly obtained by photolithography process, which is expensive and time-consuming. To solve the problem mentioned above, developing a simple, cost-effective, yet efficient method to get the microstructures is necessary.

Nature has developed various materials with different microstructures in the process of evolution, which can motivate scientists' inspiration for materials design. Among these structures, those with hierarchical structures usually present advantageous properties. For

example, hierarchical structures on the tentacles of the octopus are of vital importance for the survival of this mollusc: the hierarchical structures on the tentacles are used to catch prey and for locomotion. Hierarchical structures on the inside surface of the intestine of animals increase the surface area and realize an easy absorption of nutrition. These hierarchical microstructures in biological materials have inspired the design of artificial hierarchically microstructured materials with superior properties. For example, artificial microstructured materials with superhydrophobic surfaces have been developed by mimicking the hierarchical microstructures from lotus leaves.[42] Recently, these hierarchical microstructures from nature have inspired the design of artificial hierarchical structures in the fabrication of Piezoresistive sensors. For example, bio-inspired hierarchical microstructure based Piezoresistive sensor with a linear and high sensitivity of 14 kPa^{-1} has been reported.[15] However, in this technique, the patterning procedure is sophisticated and expensive, requiring multi-steps including photolithography, selective wet etching, and high-temperature thermal oxidation. In 2015, Su et al. demonstrated a bio-inspired pressure sensor with an ultra-high sensitivity of 50.17 kPa^{-1} using natural leaves of plants as the modeling template,[39] but the fabrication process was demonstrated only in a small scale and costly electric beam evaporation was required to deposit the Ti/Au active layer. For future industrial applications, it is in demand for developing a simple, large-area-compatible, and cost-effective approach for patterning procedure to fabricate hierarchically microstructured sensing layer for high performance Piezoresistive sensors.

In line with this need, herein, we present a cost-effective and large-area-compatible strategy to fabricate graphite/PMDS composite (denoted as GPC) conducting film with bio-inspired hierarchically structured microdomes for piezoresistive pressure sensors. Commercially available sandpapers with hierarchical surface structures are introduced as the molding template to

fabricate hierarchically structured GPC film which is subsequently incorporated into pressure sensors. Compared with conventional approaches,[9,11] our proposed method is simple, cost-effective, environmental-friendly, and suitable for mass-production. The pressure sensors based on hierarchically structured GPC film exhibit a phenomenal sensitivity of 64.3 and 12.4 kPa^{-1} in the pressure range of 0-1 and 1-10 kPa, respectively. Additionally, the pressure sensors show negligible loading-unloading output signal variations after 100,000 cycles, a response time as fast as 8 ms, a low LOD of 0.9 Pa, and an excellent ambient stability of more than 1 year, which is crucial for practical applications. The high sensitivity and fast response time enable our sensors to record transient pulse waves non-invasively in real time. The pulse waves obtained by our sensors clearly reveal the widely used parameter for arterial stiffness diagnosis, demonstrating their potential for prognostication of cardiovascular diseases. As proof of concept, we further demonstrate their excellent performance in detecting acoustic vibrations, spatial pressure distribution, and subtle motions of human body.

EXPERIMENTAL SECTION

Materials. Polydimethylsiloxane (PDMS, Sylgard 184) was purchased from Dow Corning. Graphite powder with a diameter of 10-25 μm was ordered from Beijing Jinglong Tetan Technology Co., Ltd. Indium-tin oxide (ITO) coated poly(ethylene terephthalate) (PET) sheets (200 μm thick) were obtained from Sigma Aldrich. Sandpaper (120#, Flying Parrot Brand, Korea) was from supermarket. All materials were used as received without further purification.

Preparation of graphite/PMDS ink. PDMS prepolymer was prepared by mixing the base monomer with the curing agent (the weight ratio of base monomer to curing agent was 5:1), followed by thoroughly stirring with a mechanical agitator for 5 min. To prepare GPC inks with

different concentrations (5, 15, 25, 35, 45 and 55 wt%) of graphite powder, various masses of graphite powder were slowly added to 5 g PDMS prepolymer, followed by mechanical agitation for 30 min.

Fabrication of GPC film and pressure sensors. Firstly, the surface of sandpaper and PET substrate were cleaned with ethanol followed by drying with nitrogen gas. Secondly, two PET stripes (thickness ~240 μm) were attached to the edges of the sandpaper with assistance of polyimide (PI) tape to define the thickness of GPC film. Thirdly, GPC ink was casted onto sandpaper mold template and ITO-coated PET (ITO/PET) film was laminated on top (the ITO side faced the ink). Then, roller-bar-assisted pressing was carried out to help to form a uniform film between sandpaper and ITO/PET film. After that, the sample was sandwiched between two steel plates and thermally annealed at 90 ^{o}C for 1 h to solidify the composite film. The steel plates were employed to avoid the deformations of PET and sandpaper in the process of thermal annealing. The hierarchically structured GPC film on ITO/PET film was obtained after careful peeling off from sandpaper. Finally, the composite film was cut into proper size and two pieces of the composite films with hierarchical structures were placed face-to-face, with copper wires connecting to the edge of ITO-coated side to form the electrodes, achieving flexible pressure sensors. The overall fabrication procedure was depicted in Figure 1a. The fabrication procedure of flat GPC film and pressure sensor based on flat GPC film was similar with the hierarchically structured ones except that the flat GPC film was fabricated on a PET sheet instead of sandpaper mold.

Fabrication of the pressure sensor arrays. Firstly**,** the as prepared GPC conductive film was cut into small pieces (5 × 5 mm^2), followed by transferring to clean ITO/PET stripes (60 × 5 mm^2) with tweezers. Then copper wires were connected to every bar of the ITO/PET with

conductive tape and a conventional crossbar configuration was employed to form the pressure sensor arrays (Figure 7).

Characterization of the GPC film. The morphology of graphite powder was characterized by scanning electron microscopy (SEM, 15 kV, JEOL, JSM-6490), and the crystal structures were characterized by X-ray diffractometer (XRD, Bruker, D8 Phaser) using Cu Kα radiation (λ =1.5418 Å) and Raman Spectroscopy (Reishaw 2000). The surface microstructures and cross-section of hierarchically structured graphite/PDMS films, and the cross-section of pristine PDMS were observed with SEM.

Performance measurements of the pressure sensor and arrays. The current responses to pressure were recorded with a computer controlled testing system including a force gauge (Mark-10) and motorized test stand (Mark-10). For the long-term durability measurement of devices, the current changes are measured for every 20,000 loading/unloading cycles and a dataset of 200 cycles are presented in every recording under a pressure of 1 kPa and a frequency of 1 Hz. For monitoring the wrist pulses before (normal condition) and after physical exercise, the pressure sensor has been fixed on the wrist artery of a volunteer with the assistance of PI tape. For data collection, the sensor was attached on the wrist during the whole process and then stopped to measure the signals of wrist pulses without rest. For the acoustic vibration pressure sensing, the sensor was affixed onto the speaker which was connected to a laptop. For the ambient stability measurement, the sensor was exposed in ambient condition without any capsulation for 1 year, and then the sensor was attached to the same volunteer's wrist to measure the pulse signals. The applied voltage between two electrodes was 1 V and all the current-time characteristics were recorded by the Agilent 4155C Semiconductor Parameter Analyzer in ambient condition.

RESULTS AND DISCUSSION

Device Fabrication

Commercially available graphite powder and sandpaper are employed as the conductive component and molding template, respectively, for fabrication of the bio-inspired, hierarchically structured GPC film. The optical image and the characterization of the graphite powder are depicted in Figure S1 (Supporting Information). The overall fabrication procedures of a hierarchically structured GPC film and pressure sensor are illustrated in Figure 1a. First, the PDMS elastomer and its corresponding curing agent are mixed thoroughly with a mass ratio of 5:1. Second, the graphite powder is slowly added into the PDMS solution with a graphite concentration of 45 weight percent (wt %) and stirred for 30 minutes by mechanical agitation. Third, the mixed composite ink is then drop-casted onto the sandpaper to create hierarchically structured surface. Fourth, an indium-tin oxide (ITO) on poly(ethylene terephthalate) (PET) film is laminated above the ink (the ITO side faced the ink) consisting of two thin PET strips as spacers for defining the thickness of the fabricated GPC film. Fifth, a roller-bar-assisted pressing is carried out to ensure the formation of a uniform film, sandwiched between the sandpaper and the ITO/PET film. Sixth, the sample is thermally annealed at 90 ^{o}C for 1 h to solidify the composite film. Seventh, the hierarchically structured GPC film on ITO/PET film is obtained after carefully peeling off from the sandpaper (see the optical image in Figure 1b). Finally, the hierarchically structured GPC films on ITO/PET substrate are assembled into pressure sensors (see the optical image of the pressure sensor in inset of Figure 1b). The scanning electron microscopy (SEM) images of the sandpaper template are shown in Figure 1c and d, indicating the hierarchical structures of the template. Figure 1e shows the cross-sectional SEM image of the GPC film. In contrast with the pristine PDMS film, the graphite fillers are well confined by the

PDMS elastomer and the GPC film has a thickness around 282 μm (Figure 1e and Supplementary Figure S2). Moreover, the top-view of the GPC film is also observed to

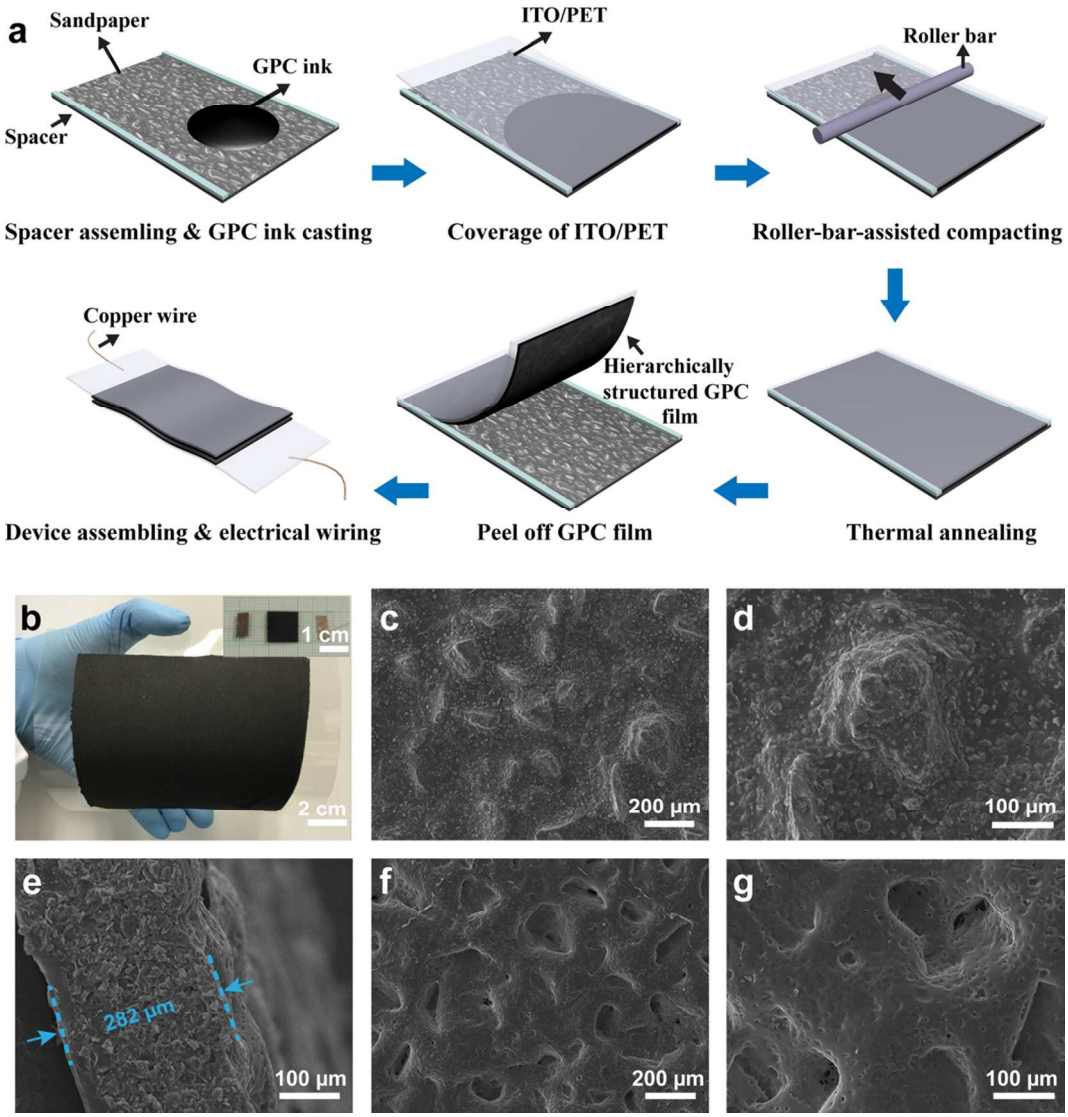

Figure 1. (a) Schematic illustration showing the fabrication procedure of GPC pressure sensor. (b) Photograph of the flexible GPC film on PET substrate. Inset: a flexible pressure sensor on PET substrate. (c), (d) SEM images showing the surface morphology of the sandpaper mold template in different magnifications. (e) Cross-sectional view of the GPC film showing the thickness. (f), (g) SEM images showing the hierarchically structured surface of the GPC film molded from the sandpaper.

investigate the surface morphologies (Figure 1f and g). Notably, the GPC film could well replicate the surface structures of the sandpaper template. It is also observed that the diameter of the large caverns is approximately 150 ± 50 μm and the diameter of the observed subtle caverns on surface is approximately 10 ± 5 μm. In consideration of the diameters of the subtle and large caverns, the microstructure could be modeled as a hierarchical structure. The piezoresistive pressure sensor device is then formed from two pieces of hierarchically structured GPC film as shown in Figure 1a. Two pieces of GPC film (the area of GPC film is 1 × 1 cm^2) on ITO/PET substrate are placed face-to-face into an interlocked construction. The copper wires are anchored onto the top and bottom ITO electrodes to form the external electrical connections. The GPC film is designed to deform due to the external pressure eventually the contact area between the top and bottom GPC films are increased. The increased contact area decreases the overall resistance, therefore the current flowing through the GPC films increases due to the applied external pressure at a given voltage. For comparison, the control pressure sensor device based on the planar GPC film is prepared and the details are described in the experimental section. Additionally, the conductivity of the composite film can be well controlled by varying the mass concentration of graphite powder in the composite film, and the related control devices have also been fabricated (see the Experimental Section) and tested.

Sensing Mechanism

The mechanism of our pressure sensor is ascribed to the pressure-dependent contact between the top and bottom hierarchically microstructured surfaces (Supplementary Figure S3). Notably, unlike the films with regular-patterned surface,[2] both the contact area and the contact pathways of these hierarchically structured GPC films increased when applied an external pressure. Without pressure, very few humps make the contact between the top and bottom layers (see

Supplementary Figure S3a), resulting in a high contact resistance between the two layers. A related equivalent circuit scheme diagram is depicted (see Supplementary Figure S3b). The total resistance (R_{Tot}) of the circuit is equal to the sum of the resistance of the top film (R_{TF}), resistance of the bottom film (R_{BF}), and the contact resistance (R_C). In comparison with the previous results on the regularly patterned structures,[2,3] without pressure, the contact area is significantly decreased and R_C is high, resulting in a small initial current, which is ideal for enhancing the sensitivity of the pressure sensors. The contact area between the top and bottom layer increases quickly when an external pressure is applied to the device, and in turn a significant resistance change is obtained (Supplementary Figure S3c and d). With a much larger external pressure, more bumps on the top and the bottom layers closely contact with each other to form more pathways, resulting in further reduced resistance and corresponding current enhancement. On unloading, these deformed structures would recover to their original shapes, and the resistance simultaneously increases to the initial value.

Sensitivity, limit of detection, and operational stability

To measure the resistance responses of our pressure sensor to the static and dynamic forces, a computer controlled testing system containing a force gauge connected to a motorized test stand and a semiconductor parameter analyzer has been used (Supplementary Figure S4). The force loaded on the sensor is preciously placed by the computer controlled force gauge and the electrical signals of the device are collected by the semiconductor parameter analyzer. As shown in Figure 2a, using the testing system (Inset of Figure 2a is the photograph of the testing system), the pressure sensitivity of the device has been measured under a wide range of applied pressures. The sensitivity S can be defined as: $S = (\Delta I/I_{off})/\Delta P$, where $\Delta I = (I_p\text{-}I_{off})$ is the current change, I_{off} is the current at the initial stage without external loaded pressure, and ΔP is the change due to

external pressure. As shown in Figure 2a, it is observed that the applied pressure influences the sensitivity and the curve could be divided into two regions based on the difference in sensitivity. In the low-pressure region (0 to 1 kPa), the sensitivity of the sensor is 64.3 kPa^{-1}, and a sensitivity of 12.4 kPa^{-1} is realized at the region of high-pressure (1 to 10 kPa). The sensitivity of our hierarchically structured sensor is higher than most of the previously reported records in flexible piezoresistive pressure sensor devices.[15,21,26] The relatively high sensitivity in this pressure range enables our proposed pressure sensors to detect the wrist pulses, acoustic vibrations, and subtle human body motions effectively. Compared with the sensors based on this type of hierarchical structure, those established on planar GPC films have a very poor sensitivity (Supplementary Figure S5a). For the control device based on the planar GPC film, more conductive pathways have been formed even without an external pressure, therefore a large I_{off} and a limited change in contact area, resulting in a poor sensitivity. Furthermore, the effect of the concentration of the conductive component on sensitivity is also investigated (Supplementary Figure S5b). When the concentration of the conductive component is less than 25 wt%, the graphite fillers are isolated from each other by the PDMS elastomer, resulting in a very high resistance and low sensitivity to the external pressure. When the concentration of the conductive fillers is 45 wt%, the pressure sensor shows the highest sensitivity. It is also observed that the sensitivity of the device decreases when the concentration of the graphite powder is further increased. This phenomenon can be explained by the increased Young's modulus of the sensing layer and correspondingly reduced flexibility when the concentration of the conductive component is further increased. Because of this, the pressure sensors are all based on 45 wt% GPC, unless otherwise stated.

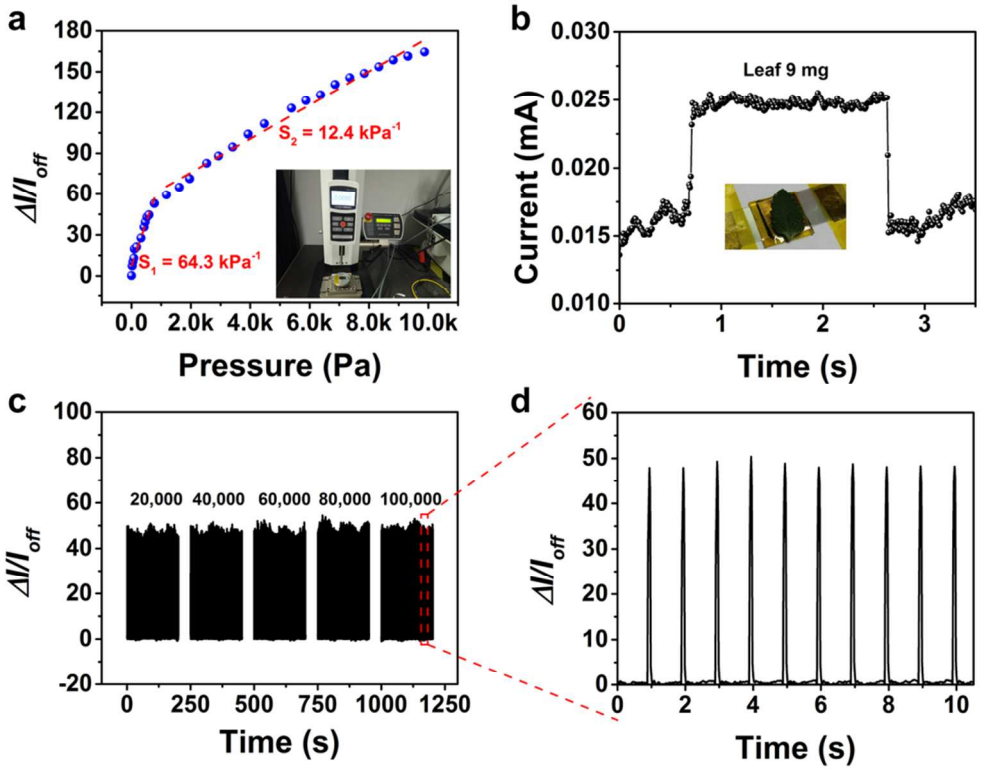

Figure 2. (a) Current responses to the pressures in the range of 0-10 kPa, showing a sensitivity of 64.3 kPa^{-1} within 1 kPa and 12.4 kPa^{-1} in larger pressure region. Inset: photograph of the test stand and the force gauge. (b) The current response of the sensor to the pressure generated by the leaf (9 mg). Inset: photograph of the leaf on pressure sensor. (c) The durability test under a pressure of 1 kPa at a frequency of 1 Hz for 100,000 loading/unloading cycles. The changes in current are recorded after each 20,000 cycles and a dataset of 200 cycles are presented in each recording. (d) A part of the I-t curve is enlarged from figure c after 100,000 loading/unloading cycles.

To prove the LOD of the sensor, the current responses are measured by loading/removal a small piece of plant leaf (9 mg; Figure 2b and inset of Figure 2b). Attractively, the device immediately responses to the subtle pressure change (~0.9 Pa) at 1 V as a supply voltage; and the LOD is comparable with that in previously reported studies. For example, the sensor with a sensing layer

of carbonized silk nanofiber membrane[36] achieved a LOD of 0.8 Pa, and another one with microstructured conducting composites displayed a LOD of 1 Pa.[15]

The long-term durability of the pressure sensor was investigated at 1 Hz under a loaded pressure of 1 kPa (Figure 2c). A high signal to noise ratio is observed and the current amplitude scarcely changed upon a prolonged process of 100,000 loading-unloading cycles. Figure 2d shows the magnified curves of the loading-unloading cycles at the ending stage of the long-term testing, and a negligible hysteresis is observed, indicating an excellent durability and fast response to the applied pressure. We may attribute the excellent durability to the stronger adhesion force between graphite and PDMS in the composite film than the previously reported structure with a conductive layer coated on a microstructured PDMS.[25,43] In our experimental design, the graphite fillers are well dispersed inside the liquid PDMS and are tightly confined by the PDMS elastomer after the composites are cured.

Frequency responses and relaxation time

To evaluate the current responses of the pressure sensor devices to the dynamic forces with different frequencies, their sensing performance has been further characterized under a pressure of 3 kPa at different frequencies of 0.5, 1, and 2 Hz. As shown in Figure 3, the output electrical signals remain stable with negligible change in magnitude at frequencies from 0.5 to 2 Hz. To know the response rate, scarce hysteresis is observed and the result indicates that the pressure sensor can monitor ultrafast pressure signals in real time. For an abrupt unloading process, the relaxation time is only 8 ms (Supplementary Figure S6) from 200 to 0 Pa, which is even smaller than that of human skin (~30 to 50 ms).[15,28] The fast response time may be attributed to the reduced viscoelastic effect and the hierarchical structures on the surface of the GPC film.[44]

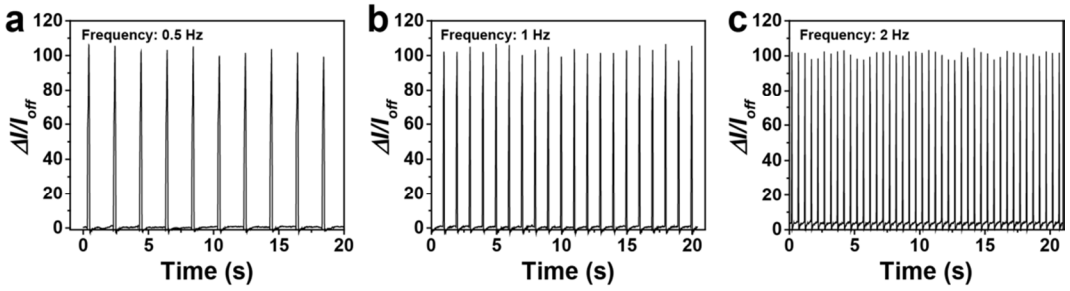

Figure 3. (a), (b) and (c) Measurements of the output signals under 3 kPa at the frequency of 0.5, 1 and 2 Hz, respectively.

Real-time healthcare monitoring

Atherosclerotic cardiovascular disease is one of the most serious diseases nowadays and can cause human death and disability. It is typically a consequence of blood vessel wall thickening and arterial stiffness change, which can be detected with the sensor by measuring the magnitude difference between the percussion waves (P-wave) and the tidal waves (T-wave). For the detection, a sensor is affixed over the radial artery of wrist with assistance of adhesive tape to demonstrate its potential applications for dynamic monitoring of human cardiovascular system (Figure 4a and Supplementary Movie 1). Figure 4b and c show the pulse waves sensed under before (normal condition) and after exercise, respectively. Under normal conditions, the wrist pulse for a person shows a regular pulse shape of 70 beats per minute (bpm). Following physical exercise, the pulse increases to 100 bpm with a change of pulse shape. As shown in Figure 4d, the radial artery pulse wave under normal condition is composed of three components: P-wave, T-wave, and D-wave (diastolic wave), where P-wave is the incident wave from the heartbeat, T-wave is the reflected wave from the hand, and D-wave the reflected wave from the lower part of human body.[45] The systolic augmentation index (AI) in the central arteries is used to diagnose arterial stiffness and is obtained from the P-wave and T-wave. The systolic AI in the central

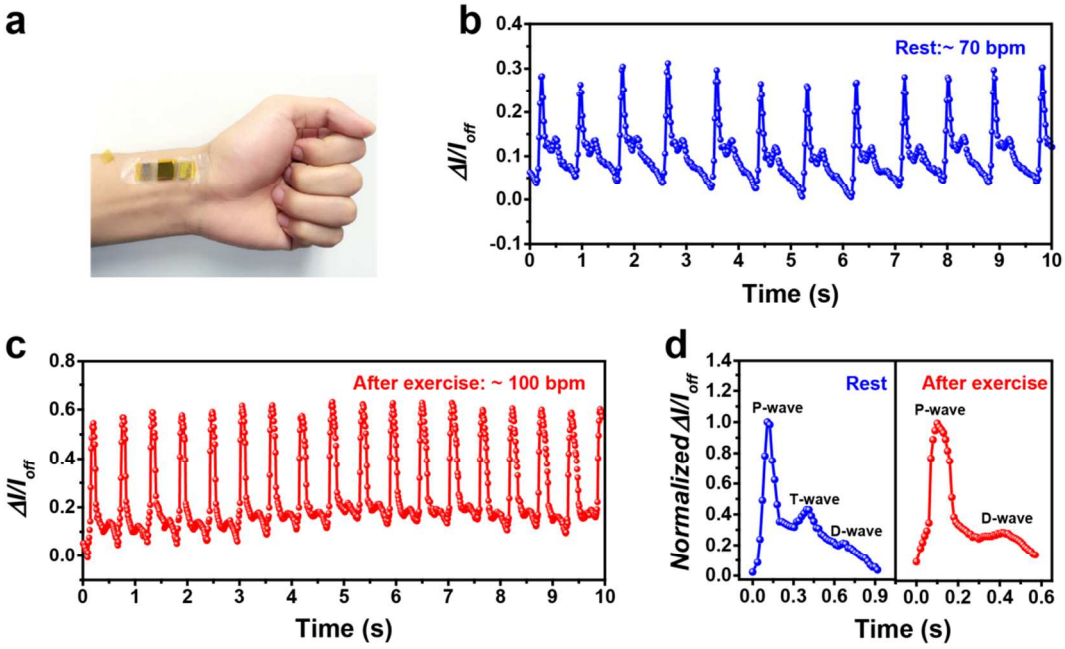

Figure 4. (a) Photograph of the sensor device fixed on the wrist. (b) and (c) Arterial pulse waves of 28-year-old male measured under normal and exercise conditions, respectively. (d) Single signal waveform extracted from (b) and (c).

arteries has direct relation with the age of people: a small AI indicates healthy blood vessels with a low stiffness. The detailed information to calculate the systolic AI is described in Supplementary Figure S7. An average AI value of a 28-year-old male volunteer is 59% from the pulse waveforms measured by our pressure sensor. This value indicates the man does not have a vascular aging problem.[46] By virtue of the good durability, fast response speed, and ultra-high sensitivity, our hierarchically structured GPC based pressure sensors are potential candidates for applications in the digital watch for noninvasive and real-time healthcare monitoring.

Detection of acoustic vibrations

Next, we further demonstrate that the hierarchically structured GPC based pressure sensors are able to detect acoustic vibrations. For this, we affix the sensor to a speaker that is connected to a

laptop (Supplementary Figure S8 and Supplementary Movie 2 and 3). Interestingly, tiny acoustic vibrations from the music could be clearly resolved (Figure 5a, b, and c). When different pieces of Chinese classical music, “CunZai” (denoted as Music 1), “ChunTianLi” (denoted as Music 2), and “JuHuaTai” (denoted as Music 3) are played, well-defined current waves have been obtained. Each piece of music is repeated for three times to investigate the reliability of the sensor.

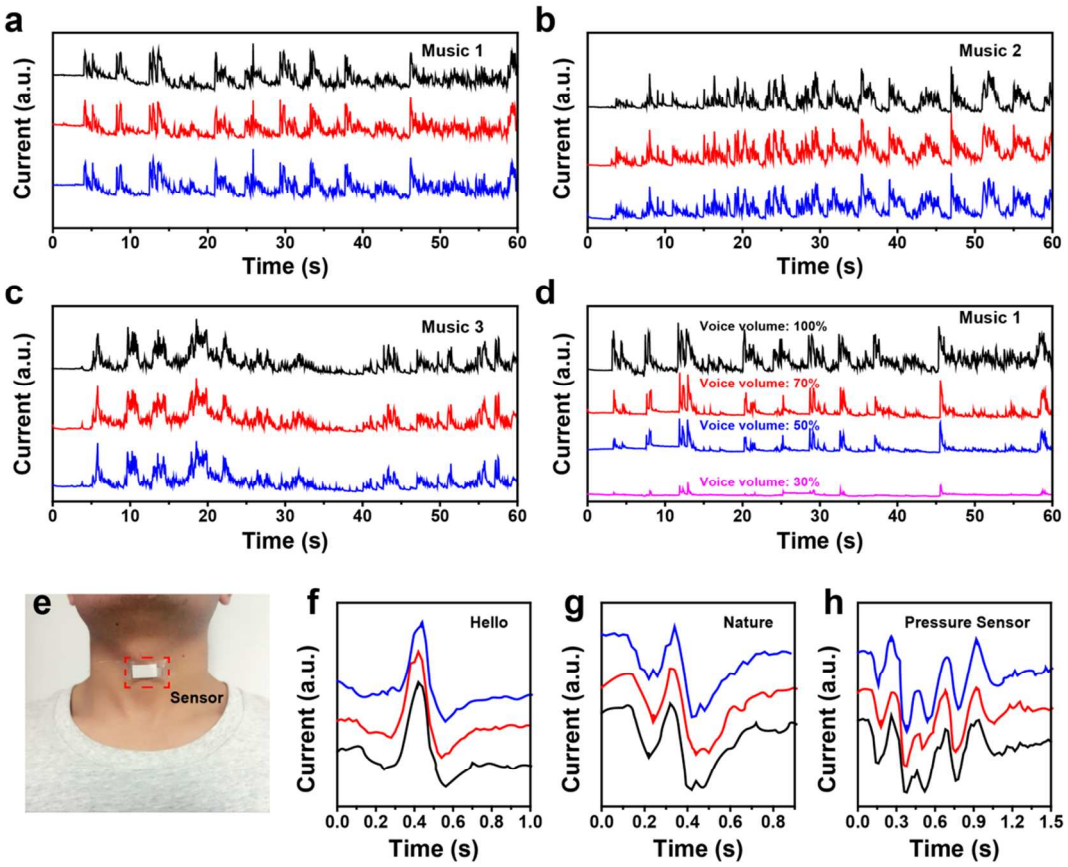

Figure 5. (a), (b),and (c) Current responses to three different pieces of Chinese classical music. Every piece of music played for three times.(d) Current responses to Music 1 and four different voice volumes (100, 70, 50, and 30%) were tested. (e) Photograph showing pressure sensor attached at the throat with assistance of woundplast for monitoring muscle movement and vibrations during speech. (f), (g), and (h) Current responses to the vibrations from different words, “Hello”, “Nature”, and “Pressure Sensor”.

Notably, the current response curves to the same music exhibit similar patterns, indicating an excellent reliability. Even when the voice volume of the music is reduced to 30%, the acoustic vibrational forces are still well detected, indicating the high sensitivity (Figure 5d and Supplementary Movie 3). For another demonstration in speech recognition, the sensor is attached to a volunteer's throat for detecting the complicated epidermis/muscle movements and acoustic vibrations during speaking. When the volunteer speaks different words and phrase, such as "Hello", "Nature", and "Pressure Sensor", distinct and repeatable patterns are obtained (Figure 5e-h). As shown in Supplementary Figure S9, these test signals are made possible by two processes: epidermis/muscle movements and acoustic vibrations, indicating that our pressure sensors could be used for voice recognition and phonation rehabilitation exercise.

Detection of subtle human body motions

The potential applications of our pressure sensors in the machine/human interface interactions are further verified by affixing the sensor to different parts of human skin (finger and face) with PI tape (Figure 6). When the pressure sensor is attached on an index finger, and a pressure is applied to the pressure sensor while the volunteer bent her index finger. Once the index finger is moved to the flat state, the pressure applied to the sensor disappears and the resistance of the sensor goes back to its initial state. Figure 6a shows the continuous current responses by repeatedly changing the states of the finger from flat to bending state, revealing that our sensor could effectively detect the states of the finger. Figure 6b illustrates the current responses of the pressure sensor attached to the face. With expansion or relaxation of the facial muscle, a pressure is loaded or unloaded, respectively, resulting in a low or high resistance simultaneously. As a consequence, the duration of expansion and relaxation of the facial muscle movement is effectively distinguished. Although the human body motion is subtle, a very high signal-to-noise

pattern is detected by our pressure sensor, which indicates the potential application in biomedical rehabilitation.

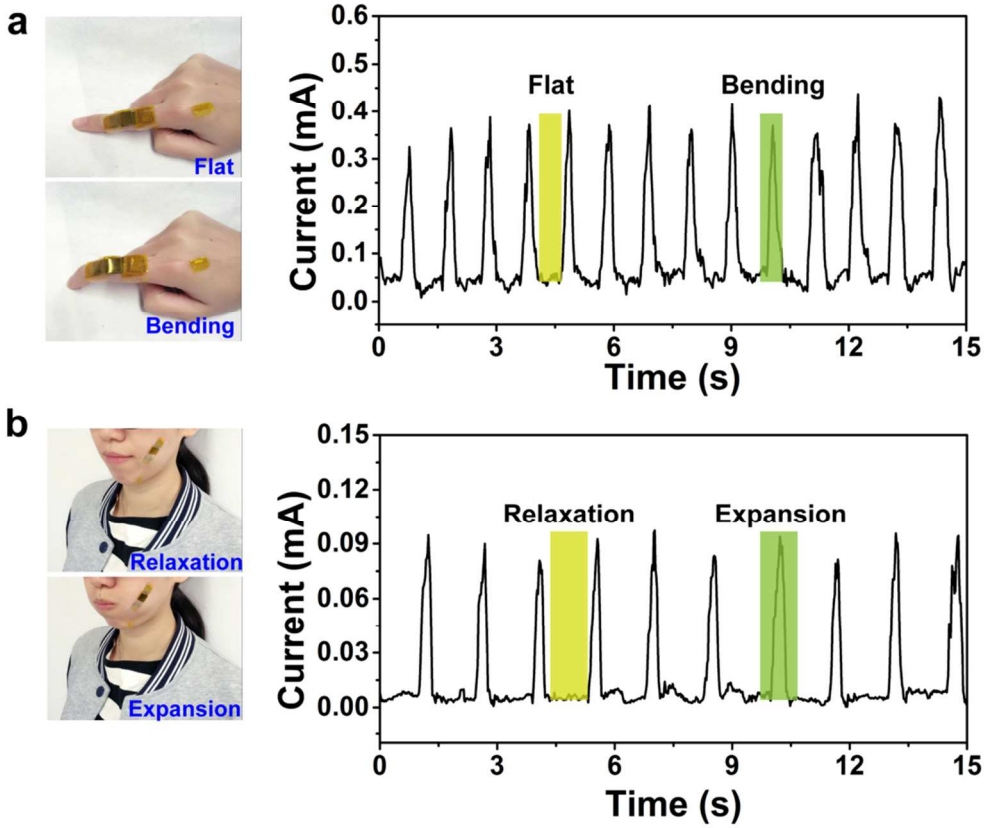

Figure 6. (a) Current responses to repetitive finger bending motion. The photograph (left) shows the states of the index finger. (b) Current responses to continuous relaxation and expansion of the facial muscle. The left photograph shows the relaxation and expansion of the facial muscle.

Detection of spatial distribution of pressure

For the practical applications of touch display and electronic skin (e-skin), there is an urgent demand to fabricate sensing arrays in large scale with a low cost. To demonstrate this, we have fabricated GPC film with hierarchical structures on PET substrate with a size of 12 × 12 cm^2. Then the film has been cut into small pieces (5 × 5 mm^2) and attached to the ITO/PET strips to form a 25 pixels sensor array using conventional crossbar configuration. Copper wires are

connected to each pixel for measurement. As shown in Figure 7a and b, without any external pressures to the pixels, all sensors show high resistance and low currents. When three different weights (1, 2, and 5 g), which are similar with gentle finger touch on human skin, are loaded on the sensor arrays (Figure 7c), the spatial distributions of pressure are clearly revealed by current mapping of sensor arrays (Figure 7d), indicating the great potential applications for e-skin.

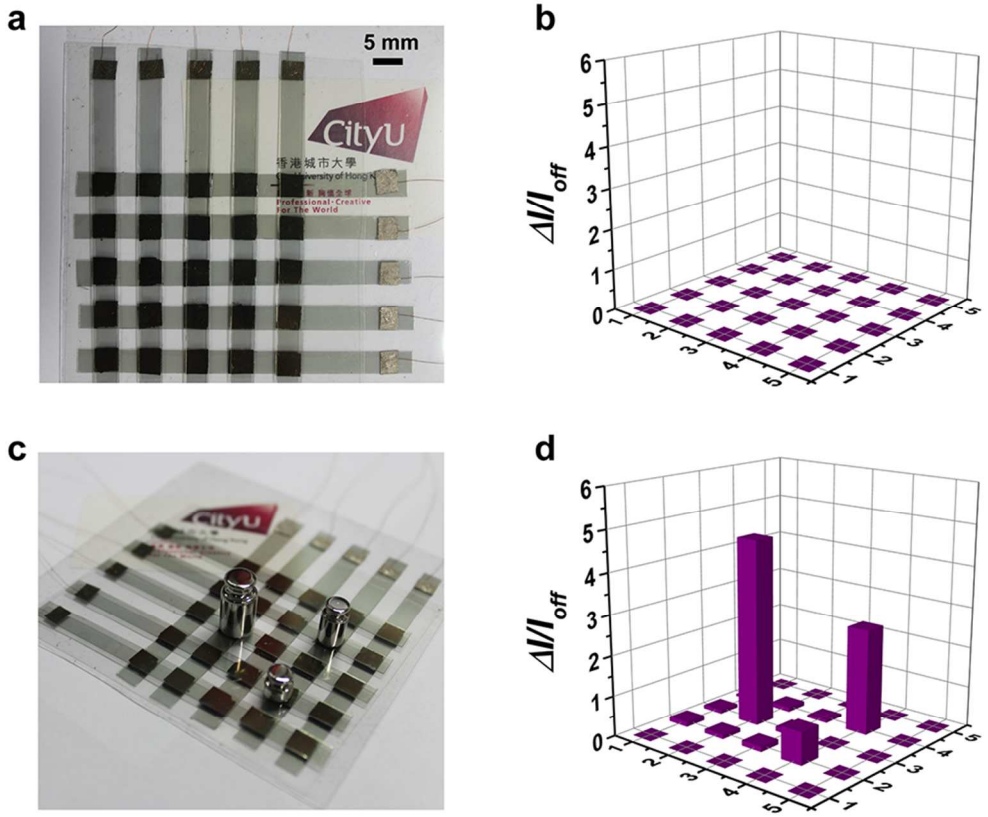

Figure 7. (a) Photographic image of large-area sensor arrays with 5 × 5 pixels. The scale bar is 5 mm. (b) The current mapping for pressure distributions in (a). (c) Photograph of the pressure sensor array with different weights (1, 2, and 5 g) distributed on the pixelated sensor arrays. (d) The current mapping for pressure distributions for the weights in (c).

Stability of hierarchically structured GPC-based pressure sensors

For practical applications in wearable electronics, an excellent stability for the pressure sensor is desired. The stability of the pressure sensor device under extreme moisture environment was

studied. The pressure sensor devices were placed in ambient condition without encapsulation package measures for 1 year (humidity > 70%) and attached to human wrist for healthcare monitoring test. As shown in Figure S10 (Supporting Information), the P-wave and D-wave could be still clearly distinguished by the sensor, indicating an excellent ambient stability of the pressure sensors. Above results indicate that our hierarchically structured GPC-based pressure sensor has the outstanding stability in moisture condition.

CONCLUSIONS

In summary, we have developed a simple, cost-effective, and large-area-compatible approach to fabricate bio-inspired, hierarchically structured GPC conducting film for highly-sensitive, fast-responsive and ultra-stable pressure sensor. These novel pressure sensors exhibit spectacular sensitivity, a rapid response time, a low LOD under a low operation voltage of 1 V. More importantly, the pressure sensors demonstrate a long-term durability of over 100,000 loading-unloading cycles and an excellent ambient stability of over 1 year. Due to outstanding sensing performance, the novel sensor is able to detect real-time human wrist pulses to monitor the cardiovascular system, which is attractive for wearable healthcare electronics applications. Additionally, they could detect force signals from acoustic vibrations, and subtle human body motions and could be integrated to make pixels sensor arrays to map spatial pressure distributions. Notably, no expensive materials and complicated equipment are required in the entire device fabrication process. We believe this work could effectively inspire the development of low-cost and high performance pressure sensors that could be integrated into various wearable and consumer electronics, such as medical diagnosis devices and e-skin.

ACKNOWLEDGEMENTS

This work was supported by the City University of Hong Kong's Applied Research Grant Project (No. 7004378), the Shenzhen Science and Technology Projects under Grant No. JCYJ20150625102943103 and the Young Innovative Talents Project of the Department of Education of Guangdong Province (No. 2015KQNCX141).

ASSOCIATED CONTENT

Supporting Information

Supporting Information Available: Detailed information (text, figures, and video) about characterization of the graphite powder and the composite films, detailed explanation of the sensing mechanism, schematic illustration of the measurement setup, characterization of the reference device, measurement of relaxation time, calculation of AI, detection of vocal vibration and muscle movement, and characterization of ambient stability. This material is available free of charge via the Internet at http://pubs.acs.org.

Figures S1-S10 (PDF)

Movie S1 (AVI)

Movie S2 (AVI)

Movie S3 (AVI)

AUTHOR INFORMATION

Corresponding Author

Tel: 86-852-34422729, Fax: 86-852-34420538

*E-mail: val.roy@cityu.edu.hk

Author Contributions

The manuscript was written through contributions of all authors. All authors have given approval to the final version of the manuscript.

Notes

The authors declare no competing financial interest.

ACKNOWLEDGMENT

This work was supported by the City University of Hong Kong's Applied Research Grant Project (No. 7004378), the Shenzhen Science and Technology Projects under Grant No. JCYJ20150625102943103 and the Young Innovative Talents Project of the Department of Education of Guangdong Province (No. 2015KQNCX141).

REFERENCES

(1) Kim, D. H.; Lu, N.; Ma, R.; Kim, Y. S.; Kim, R. H.; Wang, S.; Wu, J.; Won, S.; Hu, T.; Islam, A.; Yu, K.; Kim, T.; Chowdhury, R.; Ying, M.; Xu, L.; Li, M.; Chung, H.; Keum, H.; McCormick, M.; Liu, P.; Zhang, Y.; Omenetto, F. G.; Huang, Y.; Coleman, T.; Rogers, J. A.; Epidermal Electronics. *Science* **2011,** *333*, 838-843.

(2) Mannsfeld, S. C.; Tee, B. C.; Stoltenberg, R. M.; Chen, C. V.; Barman, S.; Muir, B. V.; Sokolov, A. N.; Reese, C.; Bao, Z. Highly sensitive flexible pressure sensors with microstructured rubber dielectric layers. *Nat. Mater.* **2010,** *9*, 859-864..

(3) Someya, T.; Sekitani, T.; Iba, S.; Kato, Y.; Kawaguchi, H.; Sakurai, T. A large-area, flexible pressure sensor matrix with organic field-effect transistors for artificial skin applications. *Proc. Natl. Acad. Sci. U. S. A.* **2004,** *101*, 9966-9970.

(4) Takei, K.; Takahashi, T.; Ho, J. C.; Ko, H.; Gillies, A. G.; Leu, P. W.; Fearing, R. S.; Javey, A. Nanowire active-matrix circuitry for low-voltage macroscale artificial skin. *Nat. Mater.* **2010,** *9*, 821-826.

(5) Song, J.-K.; Son, D.; Kim, J.; Yoo, Y. J.; Lee, G. J.; Wang, L.; Choi, M. K.; Yang, J.; Lee, M.; Do, K.; Koo, J. H.; Lu, N.; Kim, J. H.; Hyeon, T.; Song, Y. M.; Kim, D.-H. Wearable Force Touch Sensor Array Using a Flexible and Transparent Electrode. *Adv. Funct. Mater.* **2017,** *27*, 1605286.

(6) Wang, X.; Dong, L.; Zhang, H.; Yu, R.; Pan, C.; Wang, Z. L. Recent Progress in Electronic Skin. *Adv. Sci.* **2015,** *2*, 1500169.

(7) Larson, C.; Peele, B.; Li, S.; Robinson, S.; Totaro, M.; Beccai, L.; Mazzolai, B.; Shepherd, R. Highly stretchable electroluminescent skin for optical signaling and tactile sensing. *Science* **2016,** *351,* 1071.

(8) Boutry, C. M.; Nguyen, A.; Lawal, Q. O.; Chortos, A.; Rondeau-Gagne, S.; Bao, Z. A Sensitive and Biodegradable Pressure Sensor Array for Cardiovascular Monitoring. *Adv. Mater.* **2015,** *27*, 6954-6961.

(9) Chen, S.; Zhuo, B.; Guo, X. Large Area One-Step Facile Processing of Microstructured Elastomeric Dielectric Film for High Sensitivity and Durable Sensing over Wide Pressure Range. *ACS Appl. Mater. Interfaces* **2016,** *8*, 20364-20370.

(10) Gerratt, A. P.; Michaud, H. O.; Lacour, S. P. Elastomeric Electronic Skin for Prosthetic Tactile Sensation. *Adv. Funct. Mater.* **2015,** *25*, 2287-2295.

(11) Joo, Y.; Byun, J.; Seong, N.; Ha, J.; Kim, H.; Kim, S.; Kim, T.; Im, H.; Kim, D.; Hong, Y. Silver nanowire-embedded PDMS with a multiscale structure for a highly sensitive and robust flexible pressure sensor. *Nanoscale* **2015,** *7*, 6208-6215.

(12) Kim, S. Y.; Park, S.; Park, H. W.; Park, D. H.; Jeong, Y.; Kim, D. H. Highly Sensitive and Multimodal All-Carbon Skin Sensors Capable of Simultaneously Detecting Tactile and Biological Stimuli. *Adv. Mater.* **2015,** *27*, 4178-4185.

(13) Kwon, D.; Lee, T. I.; Shim, J.; Ryu, S.; Kim, M. S.; Kim, S.; Kim, T. S.; Park, I. Highly Sensitive, Flexible, and Wearable Pressure Sensor Based on a Giant Piezocapacitive Effect of Three-Dimensional Microporous Elastomeric Dielectric Layer. *ACS Appl. Mater. Interfaces* **2016,** *8*, 16922-16931.

(14) Li, T.; Luo, H.; Qin, L.; Wang, X.; Xiong, Z.; Ding, H.; Gu, Y.; Liu, Z.; Zhang, T., Flexible Capacitive Tactile Sensor Based on Micropatterned Dielectric Layer. *Small* **2016,** *12,* 5042-5048.

(15) Bae, G. Y.; Pak, S. W.; Kim, D.; Lee, G.; Kim, D. H.; Chung, Y.; Cho, K. Linearly and Highly Pressure-Sensitive Electronic Skin Based on a Bioinspired Hierarchical Structural Array. *Adv. Mater.* **2016,** *28,* 5300-5306.

(16) Gong, S.; Lai, D. T.; Wang, Y.; Yap, L. W.; Si, K. J.; Shi, Q.; Jason, N. N.; Sridhar, T.; Uddin, H.; Cheng, W. Tattoolike Polyaniline Microparticle-Doped Gold Nanowire Patches as Highly Durable Wearable Sensors. *ACS Appl. Mater. Interfaces* **2015,** *7,* 19700-19708.

(17) Gong, S.; Schwalb, W.; Wang, Y.; Chen, Y.; Tang, Y.; Si, J.; Shirinzadeh, B.; Cheng, W. A wearable and highly sensitive pressure sensor with ultrathin gold nanowires. *Nat. Commun.* **2014,** *5,* 3132.

(18) Han, X.; Chen, X.; Tang, X.; Chen, Y.-L.; Liu, J.-H.; Shen, Q.-D. Flexible Polymer Transducers for Dynamic Recognizing Physiological Signals. *Adv. Funct. Mater.* **2016,** *26,* 3640-3648.

(19) Jian, M.; Xia, K.; Wang, Q.; Yin, Z.; Wang, H.; Wang, C.; Xie, H.; Zhang, M.; Zhang, Y. Flexible and Highly Sensitive Pressure Sensors Based on Bionic Hierarchical Structures. *Adv. Funct. Mater.* **2017,** *27,* 1606066.

(20) Lee, D.; Lee, H.; Jeong, Y.; Ahn, Y.; Nam, G.; Lee, Y. Highly Sensitive, Transparent, and Durable Pressure Sensors Based on Sea-Urchin Shaped Metal Nanoparticles. *Adv. Mater.* **2016,** *28,* 9364-9369.

(21) Lou, Z.; Chen, S.; Wang, L.; Jiang, K.; Shen, G. An ultra-sensitive and rapid response speed graphene pressure sensors for electronic skin and health monitoring. *Nano Energy* **2016,** *23,* 7-14.

(22) Luo, N.; Dai, W.; Li, C.; Zhou, Z.; Lu, L.; Poon, C. C. Y.; Chen, S.-C.; Zhang, Y.; Zhao, N. Flexible Piezoresistive Sensor Patch Enabling Ultralow Power Cuffless Blood Pressure Measurement. *Adv. Funct. Mater.* **2016,** *26,* 1178-1187.

(23) Park, M.; Park, Y. J.; Chen, X.; Park, Y. K.; Kim, M. S.; Ahn, J. H. MoS_2-Based Tactile Sensor for Electronic Skin Applications. *Adv. Mater.* **2016,** *28,* 2556-2562.

(24) Shin, K.-Y.; Lee, J. S.; Jang, J. Highly sensitive, wearable and wireless pressure sensor using free-standing ZnO nanoneedle/PVDF hybrid thin film for heart rate monitoring. *Nano Energy* **2016,** *22,* 95-104.

(25) Wang, X.; Gu, Y.; Xiong, Z.; Cui, Z.; Zhang, T. Silk-molded flexible, ultrasensitive, and highly stable electronic skin for monitoring human physiological signals. *Adv. Mater.* **2014,** *26,* 1336-1342.

(26) Wei, Y.; Chen, S.; Lin, Y.; Yang, Z.; Liu, L. Cu–Ag core–shell nanowires for electronic skin with a petal molded microstructure. *J. Mater. Chem. C* **2015,** *3,* 9594-9602.

(27) Dagdeviren, C. *et al.* Conformable amplified lead zirconate titanate sensors with enhanced piezoelectric response for cutaneous pressure monitoring. *Nat. Commun.* **5,** 4496 (2014).

(28) Wu, W.; Wen. X.; Wang, Z. Taxel-Addressable Matrix of Vertical-Nanowire Piezotronic Transistors for Active and Adaptive Tactile Imaging. *Science* **2013,** *340,* 952-957.

(29) Chortos, A.; Liu, J.; Bao, Z. Pursuing prosthetic electronic skin. *Nat. Mater.* **2016,** *15,* 937-950.

(30) Ho, D. H.; Sun, Q.; Kim, S. Y.; Han, J. T.; Kim, D. H.; Cho, J. H. Stretchable and Multimodal All Graphene Electronic Skin. *Adv. Mater.* **2016,** *28,* 2601-2608.

(31) Kim, J.; Lee, M.; Shim, H. J.; Ghaffari, R.; Cho, H. R.; Son, D.; Jung, Y. H.; Soh, M.; Choi, C.; Jung, S.; Chu, K.; Jeon, D.; Lee, S. T.; Kim, J. H.; Choi, S. H.; Hyeon, T.; Kim, D. H. Stretchable silicon nanoribbon electronics for skin prosthesis. *Nat. Commun.* **2014,** *5,* 5747.

(32) Lee, J.; Kwon, H.; Seo, J.; Shin, S.; Koo, J. H.; Pang, C.; Son, S.; Kim, J. H.; Jang, Y. H.; Kim, D. E.; Lee, T. Conductive fiber-based ultrasensitive textile pressure sensor for wearable electronics. *Adv. Mater.* **2015,** *27,* 2433-2439.

(33) Lee, T.; Lee, W.; Kim, S.-W.; Kim, J. J.; Kim, B.-S. Flexible Textile Strain Wireless Sensor Functionalized with Hybrid Carbon Nanomaterials Supported ZnO Nanowires with Controlled Aspect Ratio. *Adv. Funct. Mater.* **2016,** *26,* 6206-6214.

(34) Nie, B.; Li, R.; Cao, J.; Brandt, J. D.; Pan, T. Flexible transparent iontronic film for interfacial capacitive pressure sensing. *Adv. Mater.* **2015,** *27,* 6055-6062.

(35) Tai, Y.; Lubineau, G. Double-Twisted Conductive Smart Threads Comprising a Homogeneously and a Gradient-Coated Thread for Multidimensional Flexible Pressure-Sensing Devices. *Adv. Funct. Mater.* **2016,** *26,* 4078-4084.

(36) Wang, Q., Jian, M., Wang, C. & Zhang, Y. Carbonized Silk Nanofiber Membrane for Transparent and Sensitive Electronic Skin. *Adv. Funct. Mater.* **27,** 1605657 (2017).

(37) Wang, Y.; Wang, L.; Yang, T.; Li, X.; Zang, X.; Zhu, M.; Wang, K.; Wu, D.; Zhu, H. Wearable and Highly Sensitive Graphene Strain Sensors for Human Motion Monitoring. *Adv. Funct. Mater.* **2014,** *24,* 4666-4670.

(38) Kim, D. I.; Trung, T. Q.; Hwang, B. U.; Kim, J. S.; Jeon, S.; Bae, J.; Park, J. J.; Lee, N. E. A Sensor Array Using Multi-functional Field-effect Transistors with Ultrahigh Sensitivity and Precision for Bio-monitoring. *Sci. Rep.* **2015,** *5,* 12705.

(39) Su, B.; Gong, S.; Ma, Z.; Yap, L. W.; Cheng, W. Mimosa-inspired design of a flexible pressure sensor with touch sensitivity. *Small* **2015,** *11,* 1886-1891.

(40) Wang, Z.; Wang, S.; Zeng, J.; Ren, X.; Chee, A. J.; Yiu, B. Y.; Chung, W. C.; Yang, Y.; Yu, A. C.; Roberts, R. C.; Tsang, A. C.; Chow, K. W.; Chan, P. K. High Sensitivity, Wearable, Piezoresistive Pressure Sensors Based on Irregular Microhump Structures and Its Applications in Body Motion Sensing. *Small* **2016,** *12,* 3827-3836.

(41) Zhu, B.; Niu, Z.; Wang, H.; Leow, W. R.; Wang, H.; Li, Y.; Zheng, L.; Wei, J.; Huo, F.; Chen, X. Microstructured graphene arrays for highly sensitive flexible tactile sensors. *Small* **2014,** *10,* 3625-3631.

(42) Zhao, Y.; Yu, C.; Lan, H.; Cao, M.; Jiang, L. Improved interfacial floatability of superhydrophobic/superhydrophilic janus sheet inspired by lotus leaf. *Adv. Funct. Mater.* **2017**, 1701466.

(43) Bae, S.; Lee, Y.; Sharma, B. K.; Lee, H.; Kim, J.; Ahn, J. Graphene-based transparent strain sensor. *Carbon* **2013,** *51,* 236-242.

(44) Pang, C.; Lee, G.; Kim, T.; Kim, S.; Kim, H.; Ahn, S.; Suh, K. A flexible and highly sensitive strain-gauge sensor using reversible interlocking of nanofibres. *Nat. Mater.* **2012,** *11,* 795-801.

(45) Nichols, W. W. Clinical measurement of arterial stiffness obtained from noninvasive pressure waveforms. *Am. J. Hypertens.* **2005,** *18,* 3S-10S.

(46) Kohara, K.; Tabara, Y.; Oshiumi, A.; Miyawaki, Y.; Kobayashi, T.; Miki, T. Radial augmentation index: a useful and easily obtainable parameter for vascular aging. *Am. J. Hypertens.* **2005,** *18,* 11S-14S.

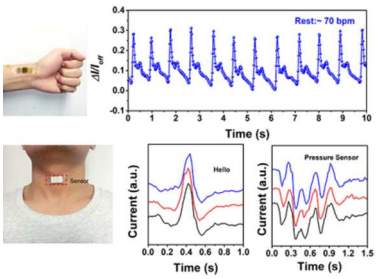

TOC graphics

(300×300 DPI)

Supplementary materials

Highly Sensitive and Ultra-Stable Skin-Sensors for Bio-Pressure and Bio-Force Measurements Based on Hierarchical Microstructures

*Qi-Jun Sun[a], Jiaqing Zhuang[a], Shishir Venkatesh[a], Ye Zhou[b], Su-Ting Han[c], Wei Wu[a], Ka-Wai Kong[d], Wen-Jung Li[d], Xianfeng Chen[e], Robert K. Y. Li[a], and Vellaisamy A. L. Roy[a]**

[a]Department of Materials Science and Engineering, City University of Hong Kong, Tat Chee Avenue, Kowloon, Hong Kong SAR, China.

[b]Institute for Advanced Study, Shenzhen University, Shenzhen 518060, P. R. China.

[c]College of Electronic Science and Technology, Shenzhen University, Shenzhen 518060, P. R. China.

[d]Department of Mechanical and Biomedical Engineering, City University of Hong Kong, Tat Chee Avenue, Kowloon, Hong Kong SAR, China.

[e]Institute for Bioengineering, School of Engineering, The University of Edinburgh, United Kingdom.
e-mail: val.roy@cityu.edu.hk.

Table of contents

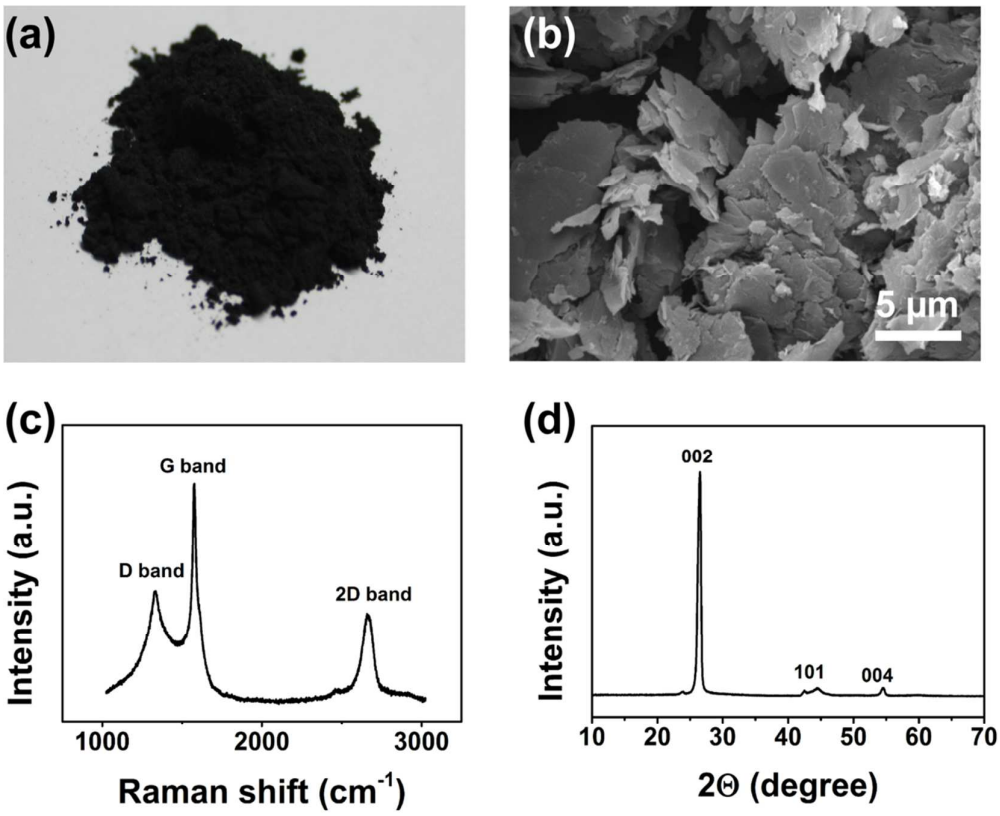

Figure S1. (a) Photograph of the graphite powder. (b) SEM image of the graphite powder. (c) Raman spectra and (d) the X-ray diffraction patterns of the graphite powder.

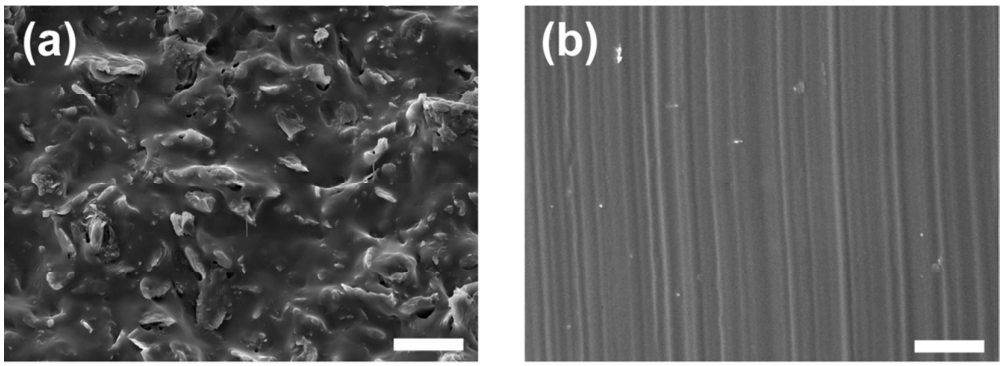

Figure S2. Cross-sectional SEM image of (a) 45 wt% GPC film and (b) the pristine PDMS film. The scale bar is 50 μm.

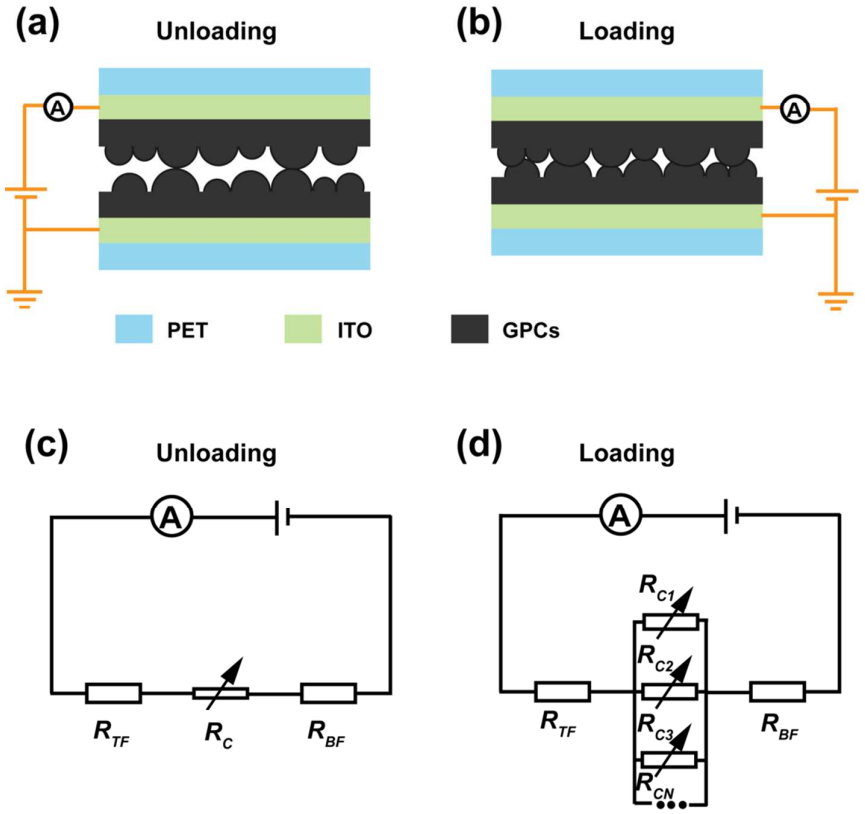

Figure S3. Sensing mechanism of the GPC pressure sensor. (a,b) Cross-sectional diagrams of the GPC pressure sensor without loading (a) and with loading (b). (c,d) are equivalent circuit diagrams of the pressure sensor without loading (a) and with loading (b). R_{TF}, R_{BF} and R_C are corresponding to the top film resistance, bottom film resistance, and the contact resistance, respectively.

Supplementary Note: Further description of the sensing mechanism.

The total resistance R_{Tot} of the circuit can be expressed as following:

$$R_{Tot} = R_{TF} + R_C + R_{BF,}$$

It should be noted that the value of contact resistance R_C is much larger than that of the film resistance (R_{TF}, R_{BF}), so the total resistance is dominated by R_C. Without pressure, there is high *Rc* between the top and bottom films, therefore a high R_{Tot} and small current when applied a voltage. With the external pressure, the beforehand contacted humps deform to obtain a larger contact area and the short humps begin to contact with each other to form more pathways, resulting in a low total resistance. Therefore, a significant resistance change is realized in comparison with that without pressure.

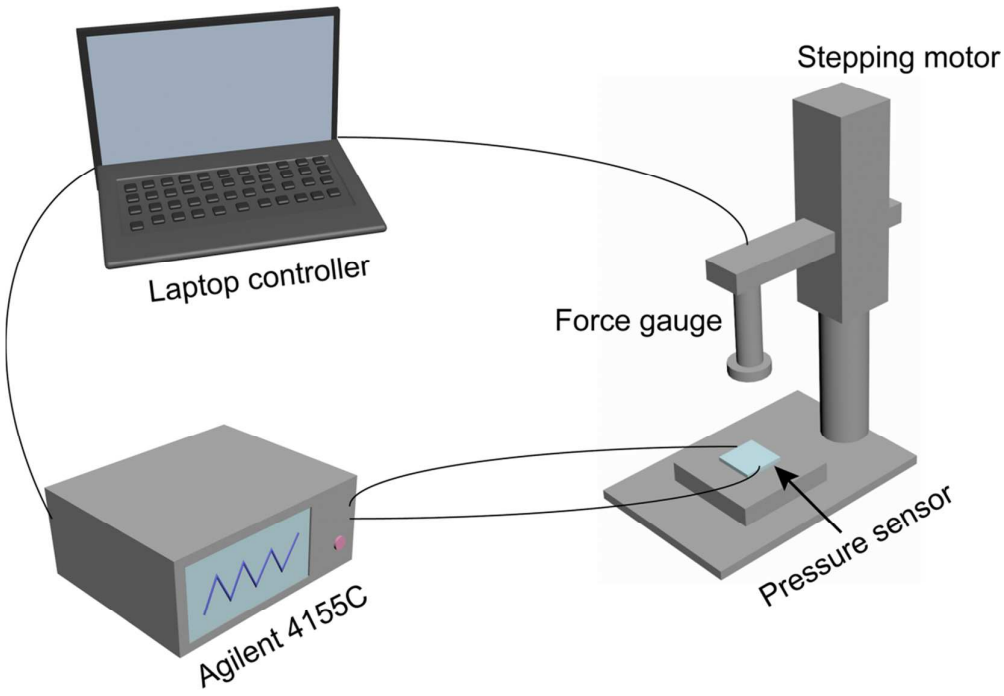

Figure S4. Schematic illustration of the measurement setup.

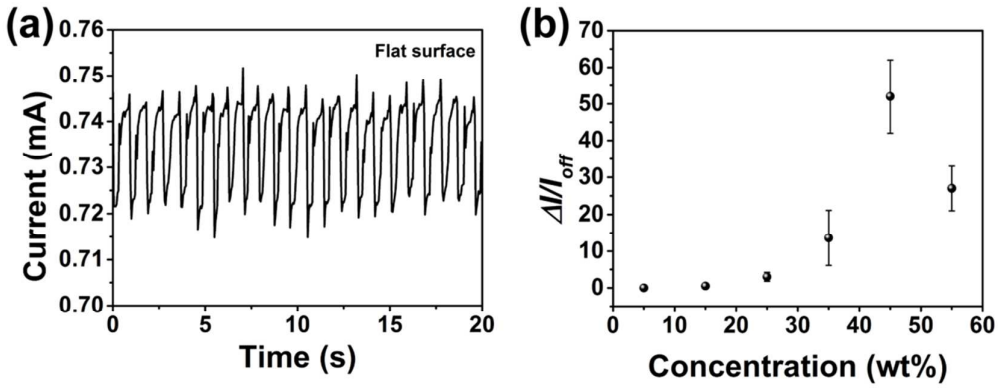

Figure S5. (a) Current responses to the loading-unloading cycles under a pressure of 1 kPa for the device based on the flat GPC film (graphite powder~45 wt%). (b) The current responses for the pressure sensors with different graphite concentrations. The loading pressure is 1 kPa.

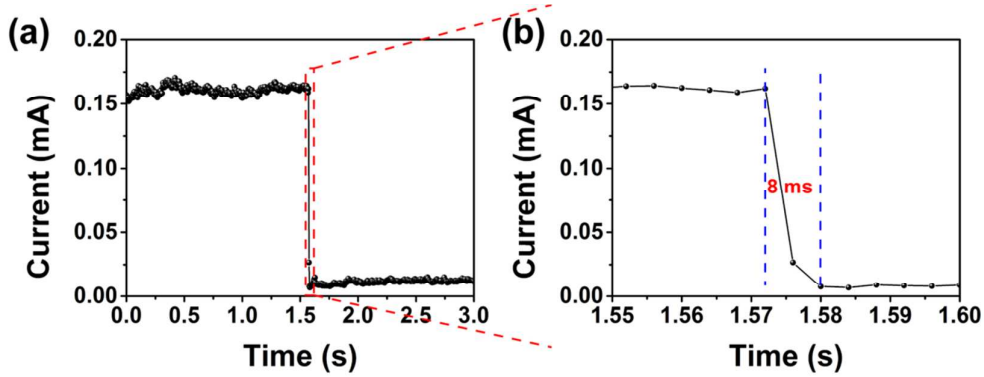

Figure S6. Current response to the abrupt unloading process from 200 to 0 Pa and the right figure shows a relaxation time within 8 ms.

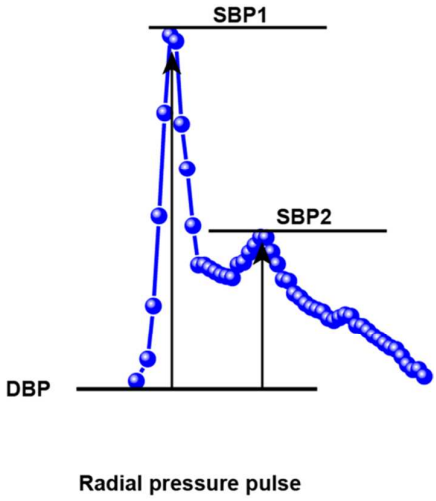

Figure S7. Calculation of AI.

Supplementary Note:

The systolic augmentation index (AI) is one of the important parameters that can suggest the health conditions of the cardiovascular system. The value of AI can be extracted by the following expression:

$$\text{Radial AI} = \frac{\text{SBP2} - \text{DBP}}{\text{SBP1} - \text{DBP}}(\%)$$

where SBP2 and SBP1 are two systolic blood pressure peaks, and DBP is the diastolic blood pressure.

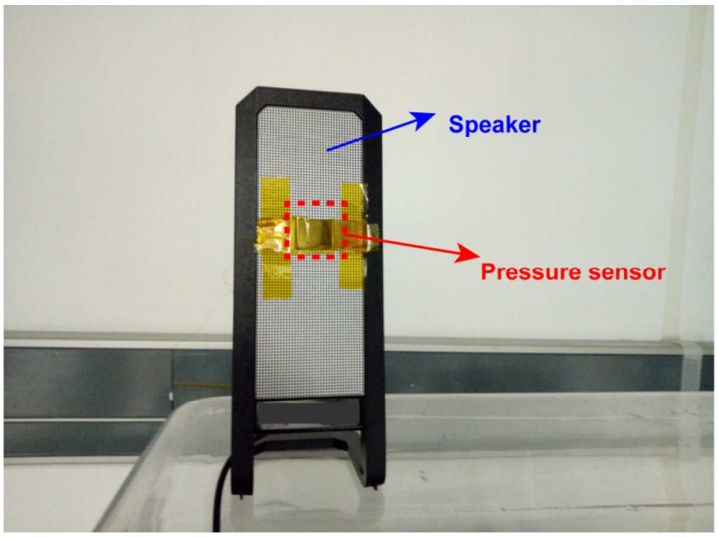

Figure S8. Photograph of the pressure sensor attached on a speaker.The pressure sensor was attached to a louder speaker with assistance of PI tape.

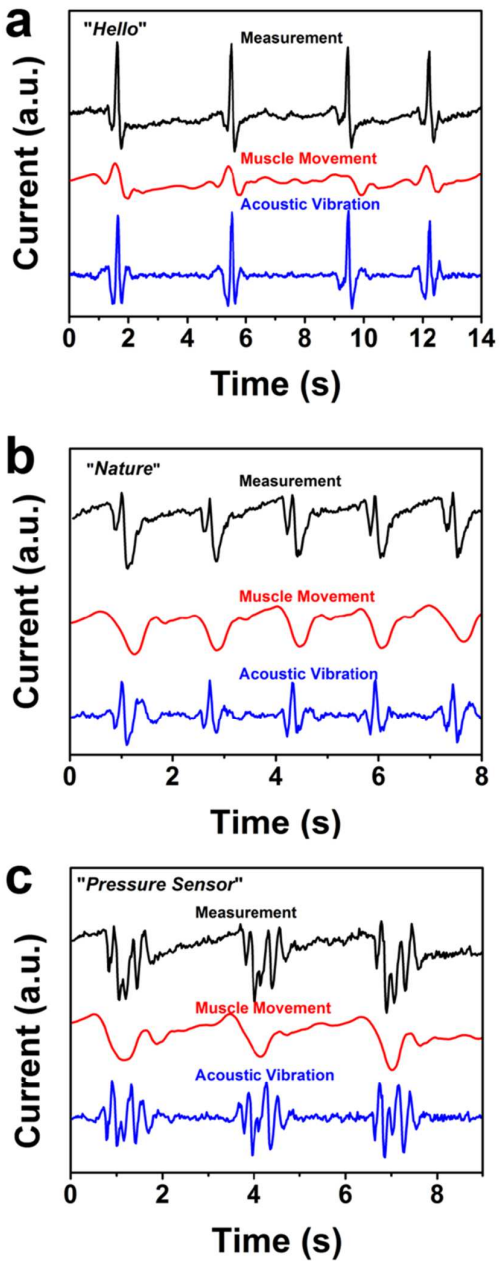

Figure S9. Detection of vocal vibration and muscle movement while speaking.

Supplementary Note:

The black curves are the measurement results while speaking "*Hello*", "*Nature*", and "*Pressure Sensor*", respectively. The recorded curves (black) are supposed to be composed of two processes: muscle movement (red) and acoustic vibration (blue), indicating the potential of our sensor for the applications in voice recognition and phonation rehabilitation exercise.

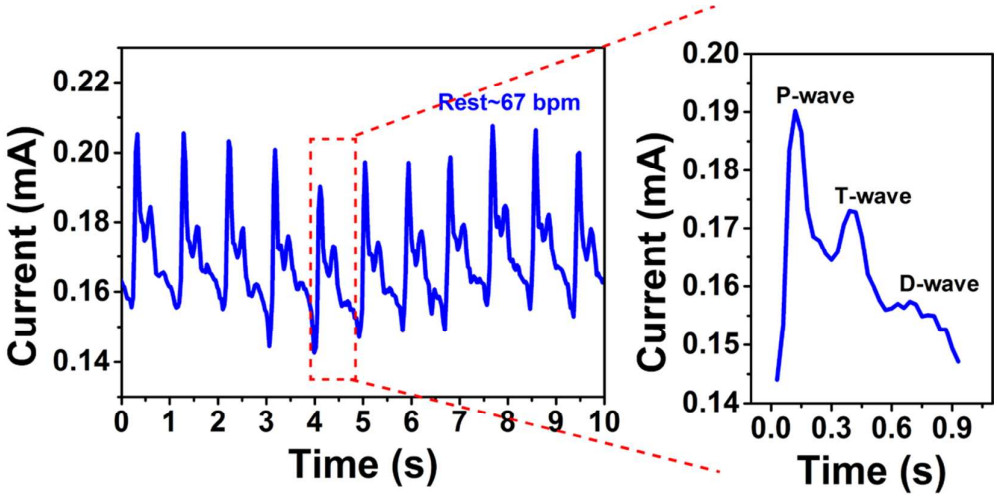

Figure S10. Arterial pulse waves under normal condition measured with the pressure sensor device stored in ambient condition for 1 year. The right figure is the enlarged view of one single pulse waveform.

Supplementary Note:

The sensor device was stored in ambient condition for 1 year without further encapsulation protection (humidity > 70%). The device was attached to the wrist of the same volunteer for the wrist pulse measurement. As shown in Figure S10, The calculated AI was 60%, which indicated that the cardiovascular system of the volunteer kept a healthy condition in the past 1 year.